Tectonics®

RESEARCH ARTICLE
10.1029/2022TC007247

Key Points:

- The best-fit solutions of most of the October 2013 and July–August 2018 foci in Lake Kinneret area span the upper 6 km
- A shallow horsetail fault pattern at a submerged tip of a plate boundary fault fits data from seismology, gravity, and field geology
- Coulomb stress calculations support triggering by the interaction of the creeping Jordan Valley Fault and the locked Jordan Gorge Fault

Supporting Information:

Supporting Information may be found in the online version of this article.

Correspondence to:

O. Barnea Cohen,
osnat.barnea@mail.huji.ac.il

Citation:

Barnea Cohen, O., Cesca, S., Dahm, T., Hofstetter, A., Hamiel, Y., & Agnon, A. (2022). Seismicity induced at the northern Dead Sea Transform Fault, Kinneret (Sea of Galilee) Basin, by shallow creep involving a salt body. *Tectonics*, *41*, e2022TC007247. https://doi.org/10.1029/2022TC007247

Received 8 FEB 2022
Accepted 24 SEP 2022

Seismicity Induced at the Northern Dead Sea Transform Fault, Kinneret (Sea of Galilee) Basin, by Shallow Creep Involving a Salt Body

O. Barnea Cohen[1], S. Cesca[2], T. Dahm[2], A. Hofstetter[3], Y. Hamiel[4], and A. Agnon[1]

[1]Neev Center for Geoinfomatics, Institute of Earth Sciences, The Hebrew University, Jerusalem, Israel, [2]GFZ German Research Center for Geoscience Potsdam, Telegrafenberg, 14473, Potsdam, Germany, [3]Independent Researcher, [4]Geological Hazards Division, Geological Survey of Israel, Jerusalem, Israel

Abstract In October 2013 and July–August 2018, two extensive earthquake swarms shook the northern reaches of Lake Kinneret (Sea of Galilee). Former studies explored the swarms, resulting in discrepant depths and mechanisms. Here, we attempt to settle the discrepant interpretations using alternative seismological methods and some unpublished data from borehole seismometers. We propose a hypothesis for the faulting phenomenon focusing on the interaction of the two plate boundary segments that step-over the northern Kinneret depocenter: a creeping segment in the south and a locked segment in the north. The energy accumulated from the interaction induces earthquake swarms from time to time. A shallow fault patch (from the surface down to 1.5 ± 1.0 km) south of the swarms is thought to creep in association with a salt formation underlying some of the basin fill. We use regional seismograms, including two near-source borehole stations, to refine the characteristics of the swarms. We test hypocentral and centroid depths using several methods and different velocity models and corroborate shallow ruptures: the majority are shallower than 6 km (all shallower than ≤10 km). The hypocentral locations and focal mechanisms suggest shallow NW-SE normal faults splaying from the tip of the creeping segment in a horsetail pattern. We test the hypothesis by Coulomb stress calculations that show stress concentration at the step-over interaction zone, consistent with focal locations and mechanisms of the earthquake swarms.

Plain Language Summary In October 2013 and July–August 2018, two unusually extensive earthquake sequences hit Lake Kinneret (Sea of Galilee). Former studies exploring the earthquakes and the active fault geometry resulted in conflicting views. Here, we investigate with alternative methods and test a new hypothesis for the driving mechanism. The study area straddles two tectonic plates joined by a segmented fault: a step-over in the northern reaches of the lake separates a southern segment continuously creeping (on the upper approximately 2 km) and a northern temporarily locked segment. The creep is thought to be associated with a flowing salt formation that underlies the lake (at a few km depths). The slip toward the locked northern segment leads to energy accumulation released by the earthquakes. We use the earthquake records to constrain source depths, the majority of which turns out to be shallower than 6 km. Moreover, source distribution and fault plane orientations suggest that they ruptured NW-SE tensional shallow faults from the northern tip of the southern segment. Gravity lineaments delineate these faults. Calculations corroborate the hypothesis predicting areas of high probability for rupture, consistent with the observed seismicity.

1. Introduction

The Dead Sea Transform Fault (Figure 1), a sinistral plate boundary (e.g., Freund et al., 1970), is longer than 1000 km and links spreading in the Red Sea with the Anatolian Fault System (Garfunkel, 1981; Sengör, 1979). The N–S-oriented fault has accumulated approximately 100 km of slip since the Neogene (Bartov et al., 1980; Garfunkel, 1981). Freund et al. (1970) and Garfunkel (1981) have suggested that an initial phase of 60 km slip involved pure transform motion, before a divergence component appeared. The southern sector of the transform is dominantly divergent with morpho-tectonic pull-apart basins (Figure 1): Gulf of Aqaba, Dead Sea, Beit Shean—Kinarot Basin, Hula Basin, and Marj 'Ayun (e.g., Ben-Avraham, 1985). Lake Kinneret (Sea of Galilee) fills the northern reaches of the Beit Shean—Kinarot Basin (Figure 2a).

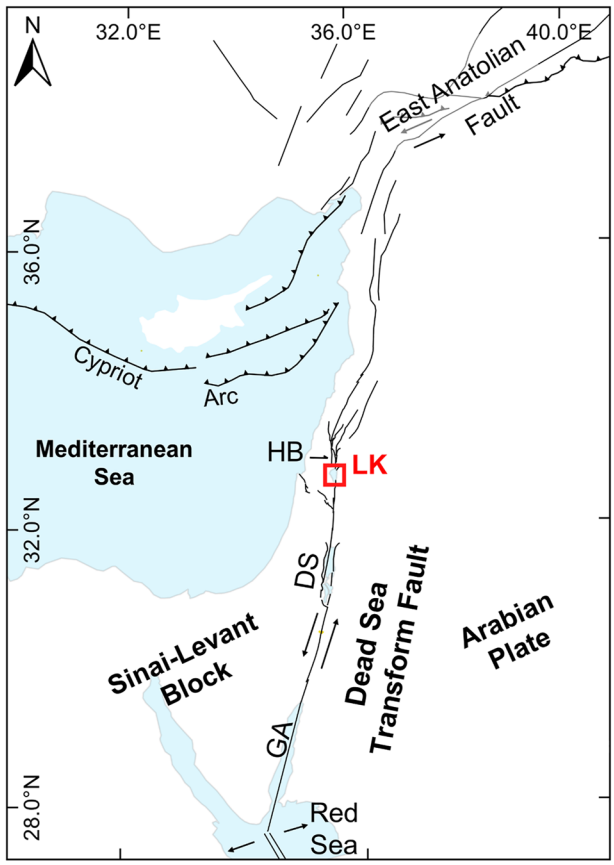

Figure 1. Regional tectonic map (faults adopted from Duman & Emre, 2013; Garfunkel et al., 1981; Sharon et al., 2020), study area marked by a red square. LK—Lake Kinneret, HB—Hula Basin, DS—Dead Sea, GA—Gulf of Aqaba.

1.1. Geological Settings

Lake Kinneret (Figure 2b) is approximately 20 km long (N–S), approximately 12 km at its widest part, with a maximum depth of approximately 40 m (Sade et al., 2009). The lake level fluctuates 210 m below mean sea level. The basin is dominated by the N–S transform strands intersected by the local NW–SE to W–E trending fault system of the Lower Galilee (Figure 2b), northwest of Lake Kinneret (e.g., Freund et al., 1970; Sneh, 2014a).

1.1.1. Onshore Dominant Fault Systems

A N–S fault duplex enters Lake Kinneret from the south (Figure 2b): the Jordan Valley Transform strand bounds the basin from the east (e.g., Hurwitz et al., 2002; Reznikov et al., 2004), and the normal Degania Fault splays from a main branch to a northwestward secondary branch. The latter curves along the shore of Lake Kinneret with strands offsetting monumental archeological edifices in Tiberias (Ferrario et al., 2020; Marco et al., 2003).

The active Jordan Gorge Transform strand (Figure 2b) extends north of the lake (Ellenblum et al., 2015; Hamiel et al., 2016; Marco et al., 2005; Wechsler et al., 2014). Together with the Jordan Valley Fault, the two strike-slip strands form a sinistral step-over with an east-west spacing of approximately 2.2 km. These dominant faults have similar slip rates (approximately 4 mm/year), with locking limited to the upper approximately 10 km (e.g., Hamiel et al., 2016; Hamiel & Piatibratova, 2021). Rotstein and Bartov (1989) presented seismic profiles with a 1–2 km wide near-surface deformation zone along the Jordan Gorge Fault near Lake Kinneret. They suggested that the Jordan Gorge Fault accommodates transpression related to push-up of Korazim Heights (Figure 2b) north of the western side of the basin.

Northeast of Lake Kinneret, the Sheikh A'li Fault (Figure 2b) diverges to the east (e.g., Michelson, 1972; Shulman et al., 2004) from the northern edge of the Jordan Valley Fault. Seismic reflection data show normal fault branches within the upper kilometers of the fault (Rotstein & Bartov, 1989; Shulman et al., 2004). On seismic images north of Lake Kinneret (Meiler et al., 2011; Rotstein & Bartov, 1989; Shulman et al., 2004), these shallow faults merge to a deeper main strand, accompanied by significant shortening structures.

1.1.2. The Complex Fault Geometry in Lake Kinneret

Previous subsurface studies used various geophysical tools (e.g., Ben-Avraham et al., 1996; Eppelbaum et al., 2007; Hurwitz et al., 2002; Tibor et al., 2004). Nevertheless, the structure of the basin and its relations to plate tectonics remain elusive. A multichannel seismic survey yielded two alternative models (Hurwitz et al., 2002; Reznikov et al., 2004) (Figures 2c and 2d). The significant difference between the two interpretations is in the western part of the lake. Hurwitz et al. (2002) continued the Degania Fault north, crossing to Korazim Heights. Reznikov et al. (2004) mapped the Degania Fault only in the southern half of Lake Kinneret and interpreted the northwestern area as very deformed. Gasperini et al. (2020) reprocessed previous data and presented another model in which two main fault systems are active (Figure 2e): (a) the marginal eastern boundary fault (the Jordan Valley Fault); (b) a putative diagonal fault (NW-SE), "Caphernaum Trough" (CT), hypothesized to splay from the Jordan Valley Fault in the southern reaches of Lake Kinneret. Then, it branches into an intricate pattern that decays onshore in the Korazim Heights. The Korazim Heights faults are mapped in detail by Belitzky (1987) and Heimann and Ron (1993).

The depocenter location is also model dependent. Ben-Avraham et al. (1996) inferred from gravity data that the depocenter is in the south-central part of Lake Kinneret (Figure 2c). Hurwitz et al. (2002) detected another depression, a half-graben, in the northern half (Figure 2c) and suggested that the modern pull-apart encloses most of Lake Kinneret in a box shape. Reznikov et al. (2004) interpreted depocenter migration to the northern reaches of the lake.

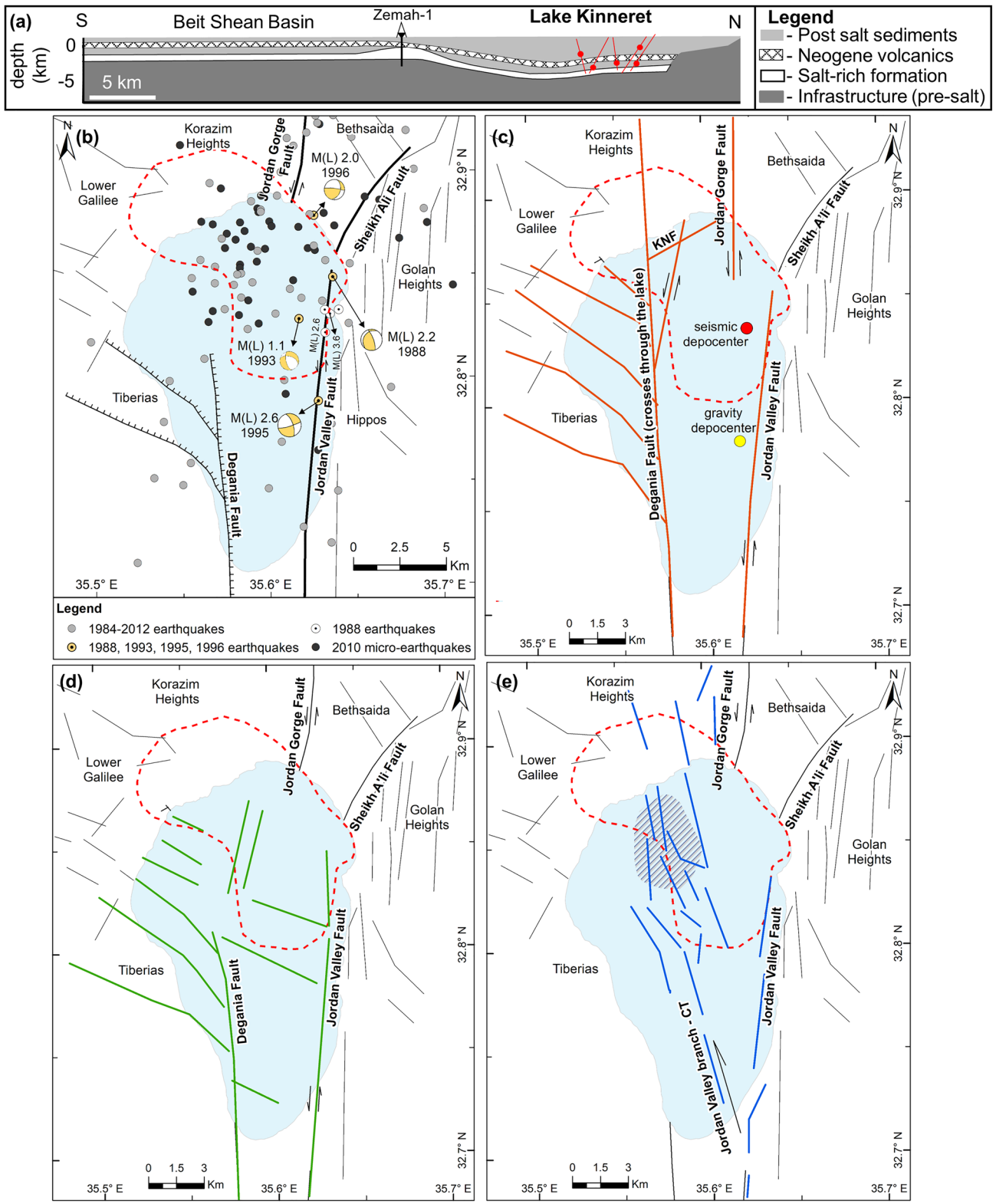
(a)
S
Beit Shean Basin
Zemah-1
Lake Kinneret
N
depth (km)
0
-5
5 km
Legend
- Post salt sediments
- Neogene volcanics
- Salt-rich formation
- Infrastructure (pre-salt)
(b)
Korazim Heights
Bethsaida
Lower Galilee
Golan Heights
Tiberias
Hippos
Jordan Gorge Fault
Sheikh A'li Fault
Jordan Valley Fault
Degania Fault
M(L) 2.0 1996
M(L) 1.1 1993
M(L) 2.6 1995
M(L) 2.2 1988
M(L) 2.6
M(L) 3.6
32.9° N
32.8° N
35.5° E
35.6° E
35.7° E
0 2.5 5 Km
Legend
1984-2012 earthquakes
1988 earthquakes
1988, 1993, 1995, 1996 earthquakes
2010 micro-earthquakes
(c)
KNF
seismic depocenter
gravity depocenter
Degania Fault (crosses through the lake)
32.7° N
0 1.5 3 Km
(d)
(e)
Jordan Valley branch - CT

Figure 2.

1.2. Pre-Instrumental Earthquakes

The study of pre-instrumental earthquakes is possible through historical documentation, archeological damage, disturbed sediments, and displaced coastal features (e.g., Agnon, 2014). Several historical earthquakes are known in Lake Kinneret area. For example, an earthquake (or more than one) from the mid-eighth century CE sequence damaged the city of Hippos (Kulat al-Hsan/Susita), east of Lake Kinneret (Figure 2b) (Marco et al., 2003). A large historic earthquake recorded on the Jordan Valley Fault (Figure 2b) ruptured the surface in 1033 CE (Ferry et al., 2011), for which Ambraseys and Jackson (1998) suggested $7.0 \leq Ms < 7.8$. North of Lake Kinneret, studies found evidence of earthquakes from 1202 ($7.6 \leq Ms \leq 7.8$, Hough & Avni, 2011), 1759, and 1837 by displacement of the walls of the Crusader castle of Vadum Iacob (Tel Ateret) (Ellenblum et al., 1998; Marco et al., 1997) approximately 16 km north of Lake Kinneret. The plates slipped, generating at least pre-Crusader three earthquakes spanning the first millennium BCE and the first millennium CE, shifting walls constructed between Iron Age to Hellenistic by a total of more than 6 m (Ellenblum et al., 2015). Trenches crossing the Jordan Gorge Fault also revealed the 1,202 and 1,759/1,837 earthquakes (Marco et al., 2005; Wechsler et al., 2014), as well as seven ruptures during the first millennium CE. The youngest pre-instrumental earthquake in Lake Kinneret area ruptured in 1837, north of the lake. It led to extensive damage in Safed (approximately 13 km NW of Lake Kinneret) and Tiberias (Figure 2b) cities, with respective estimated magnitudes of 6.5 and 7.0 (Ambraseys, 1997; Ambraseys & Barazangi, 1989). While pre-instrumental earthquakes have caused significant damage, the seismic stations in the area have not recorded earthquakes larger than M 4.5 (eq.gsi.gov.il).

1.3. The Instrumental Earthquake Record

Since the establishment of the Israel Seismic Network (ISN) in 1983, an average of 10 earthquakes per year have been recorded from Lake Kinneret area. Van-Eck and Hofstetter (1990) studied a cluster of five earthquakes from May 1988 (Figure 2b), with the highest M_L 3.6 on the Jordan Valley Fault. Hofstetter et al. (2007) derived focal mechanisms for the 1988, 1993, 1995, 1996 earthquakes. Navon (2011), using a portable local network, recorded approximately 120 micro-earthquakes in 2010 (Figure 2b).

This seismic activity is minor in Lake Kinneret compared to the Jordan Valley catalog (Wetzler & Kurzon, 2016). Quiescence was interrupted for a week in October 2013 and July–August 2018 for some 50 days by a series of earthquakes centered within the northern reaches of Lake Kinneret. Discrepant estimates of depths and mechanisms of the seismic activity lead to different interpretations. Wetzler et al. (2019) derived shallow earthquakes, <10 km depth, mostly with normal mechanisms. They suggested an anthropogenic-hydrological trigger (water pumping). Haddad et al. (2020) refined the velocity model and analyzed the 2018 earthquake records using several methods. They showed shallow normal and deep oblique strike-slip earthquakes, with hypocenters 6–13 km deep (although the centroids agree with the shallower solutions). They proposed a tectonic drive combined with mantle fluids upwelling through the transform.

1.4. Our Study

This study analyzes the near-surface ISN and Jordan Seismological Observatory (JSO) stations records of the 2013 and 2018 clusters. We also add two borehole stations, on the lake shores, for better constraining depths and mechanisms. In addition, we propose a new hypothesis for the geometry of the faults in Lake Kinneret in light of a new geodetic study that identified shallow creep (continuous aseismic slip) on the northern segment of the Jordan Valley Fault (Hamiel et al., 2016).

Figure 2. (a) A hypothetical N–S cross-section along the Beit Shean Basin integrating the gravity-based model of Rosenthal et al. (2019) and seismicity analysis by Wetzler et al. (2019). Gray colors correspond to the gravity-based model. Red circles and lines represent foci and normal faults based on relocations and mechanisms. Zemah-1 drill-hole is marked above the diapiric structure. (b) Map showing the earthquake epicenters earlier than the 2013 cluster in Lake Kinneret area. Gray circles show earthquakes located by the Israel Seismic Network (ISN) near-surface stations (eq.gsi.gov.il). Yellow circles with black dots mark Hofstetter et al.'s (2007) location and focal mechanism solutions. White circles with black dots show Van-Eck and Hofstetter's (1990) May 1988 cluster location and magnitudes. Black circles mark micro-earthquake locations calculated by Navon (2011) from March to November 2010. Dominant offshore faults are shown (e.g., Hurwitz et al., 2002; Reznikov et al., 2004; Shulman et al., 2004; Sneh & Weinberger, 2014). Normal onshore faults were adopted from Sneh (2014a, 2014b). Red-dashed curve demarcates the area of the 2013 and 2018 clusters. (c)-(e) Fault geometry in Lake Kinneret according to various studies: (c) Hurwitz et al. (2002) in orange with their interpreted seismic depocenter in red, KNF—Kfar Nahum Fault (d) Reznikov et al. (2004) in green, and (e) Gasperini et al. (2020) in blue, with their postulated "Caphernaum Trough" (CT). Proposed active deformed area is marked by slant lines in a gray oval. Also shown in (c) Ben-Avraham et al.'s (1996) depocenter location (yellow circle) inferred from gravity data.

2. Data and Methods

The seismic data of the October 2013 and July–August 2018 earthquake clusters consist of three-component records from the ISN and JSO stations (Figure 3a). Hypocenter locations are calculated using the regional velocity model of Feigin and Shapira (1994), applying automated location by waveform attribute stacking by Grigoli et al. (2013).

For improving hypocentral depth control, we assess waveforms recorded in 2018 from two borehole stations, 4.5 Hz three-component seismometers. One is at the southeastern side of Lake Kinneret, MB1I, at a borehole at 520 m depth. The second seismometer, K10B, is west of the lake at a borehole at 535 m depth (Figure 3b), merely several kilometers from the sources. Depth was also calculated for three of the largest earthquakes recorded by K10B station, using the Ts-Tp method, with Haddad et al.'s (2020) velocity model.

Point source parameters for the seven larger earthquakes, assuming a double-couple constrained moment tensor, were calculated using Cesca et al.'s (2010) method. Due to low signal-to-noise ratios, focal mechanisms are not determined for <Mw 3.3 earthquakes. We also calculated the source parameters with a full moment tensor model using a probabilistic moment tensor inversion (Heimann et al., 2018). The two models (double-couple and moment tensor) were used with four different velocity models (Gitterman et al., 2002; Haddad et al., 2020; crust_t4, http://igppweb.ucsd.edu/~gabi/rem.html; Feigin & Shapira, 1994). Note that the fitting procedure is here slightly different, as full waveforms and their amplitude spectra are fit simultaneously. The inversion procedure is accompanied by a bootstrap test on the data, which allows an estimation of source parameter uncertainties (Heimann et al., 2018).

After relocating the earthquakes and finding the focal mechanism of the larger earthquakes, we examined our hypothesis by calculating Coulomb stress change (e.g., Freed, 2005) under the Coulomb 3.3© software (www.usgs.gov). Such a mechanical model has been used for forecasting earthquake sequence zones (e.g., King et al., 1994).

3. Results

In October 2013, approximately 60 earthquakes, mainly centered in the northern reaches of Lake Kinneret (Figure 3b, Table S1 in Supporting Information S1), were recorded by the ISN and JSO stations. In July–August 2018, a cluster of approximately 660 earthquakes was recorded in the same part of Lake Kinneret but mainly clustered along a NW-SE-oriented belt (Figure 3b, Table S1 in Supporting Information S1).

We tested the hypocentral and centroid depths using different methods and several velocity models, and obtained shallow results (Figure 3b, Tables S1–S4 in Supporting Information S1). According to our relocations, about 84% of the earthquakes in 2013 and 95% in 2018 are shallow (≤6 km), with only a few reaching depths of 10 km (Table S1 in Supporting Information S1). We also selected three earthquakes of 4 July 2018, and calculated their depths using the K10B station, shallow foci, <10 km, were obtained (Table S3 in Supporting Information S1). We used another independent method to test whether all the earthquakes are shallow or some are deep, with the two borehole stations record (K10B and MB1I Figures 3a and 3b). Earthquakes from July to August 2018 are characterized by well-developed surface waves (examples in Figure S4 in Supporting Information S1). Surface wave amplitudes decrease exponentially with depth scaled to the wavelength (e.g., Kearey et al., 2002), suggesting shallow earthquakes. The periods of surface waves in Figure S4 in Supporting Information S1 range between 0.046 and 0.210 s and with a reasonable speed of 2 km/s (Ben-Gai, 2011; Reznikov et al., 2004) are 0.09–0.42 km long, supporting shallow earthquakes.

The focal mechanisms for the seven largest earthquakes, Mw 4.5-3.3, suggest shallow centroid depths (3–6 km) and normal faulting, with fault planes striking N–S and NW-SE (Figure 3b, Table S2 in Supporting Information S1 earthquakes 1–7). An additional comparison of double-couple and full moment tensor inversion solutions, using three more velocity models (Table S4, Figures S5–S7 in Supporting Information S1) confirms NW-SE striking normal faulting earthquakes. The centroid depths are, in all cases, <10 km, and most of them are ≤6 km.

Some earthquakes were relocated to the upper 0.5 km depth (Table S1 in Supporting Information S1). The shallow depths are attributed to the velocity models used, with no resolution of the upper 500 m. Moreover, there may be inaccuracies in calculations following the heterogeneous deposits and the complex geometry in the lake

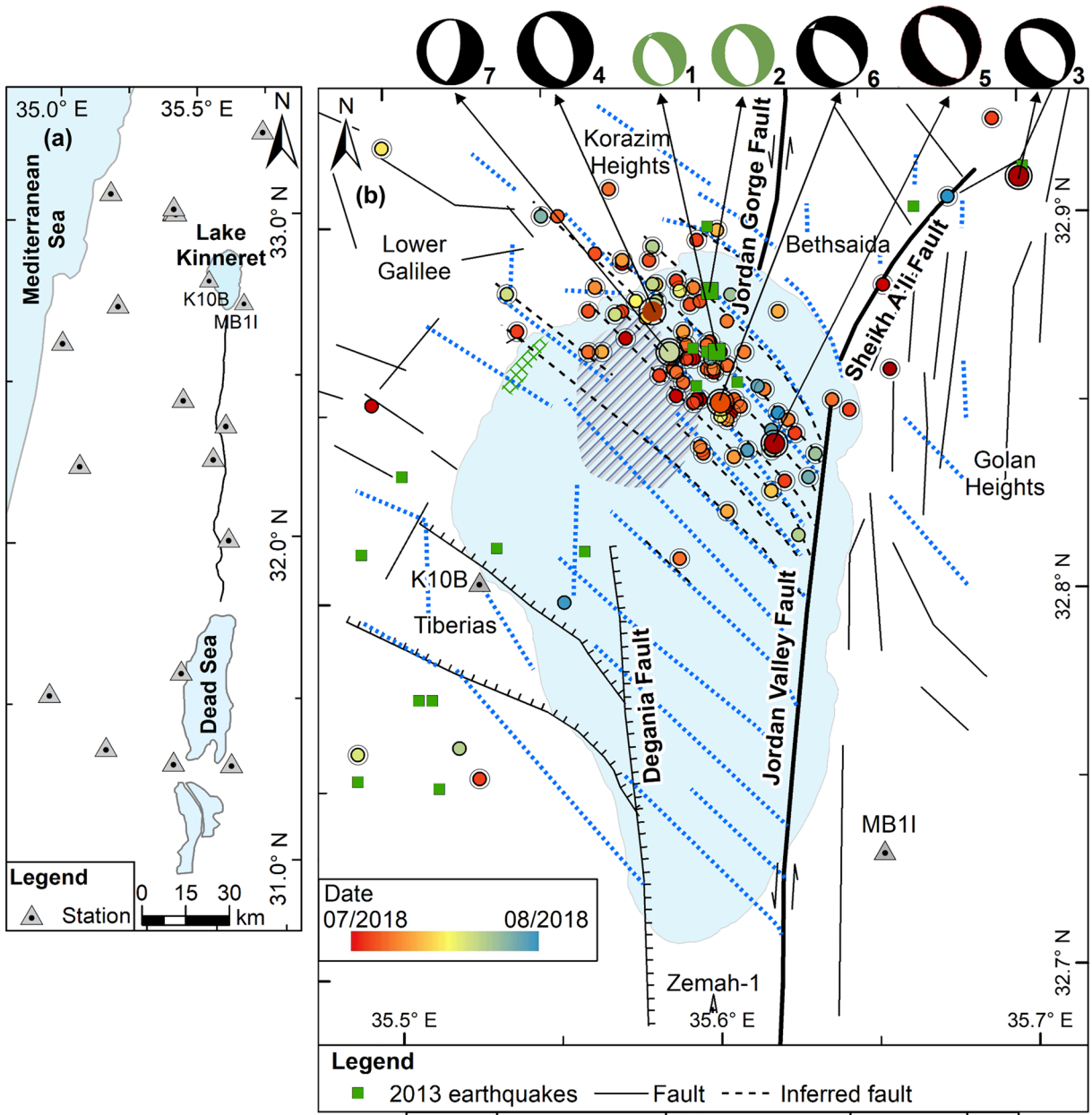

Number	Date	Time (hour:minute)	Depth (km)	Mw
1	17 October 2013	18:17	4.5	3.3
2	20 October 2013	08:50	5.8	3.6
3	4 July 2018	01:50	4.1	4.1
4	4 July 2018	03:51	5.0	3.9
5	4 July 2018	19:45	4.7	4.5
6	8 July 2018	13:30	5.1	3.9
7	27 July 2018	08:51	3.4	3.7

Figure 3. (a) The location of the ISN and the Jordan Seismological Observatory (JSO) stations used for this study. K10B and MB1I are placed in boreholes at 535 m depth and 520 m depth, respectively. (b) Fault map of Lake Kinneret and surrounding area (fault locations adopted from Hurwitz et al., 2002; Reznikov et al., 2004; Sneh, 2014b, 2014a; Sneh & Weinberger, 2014). K10B and MB1I borehole stations are shown. Relocated 2013 epicenters are marked by green squares, and circles mark the 2018 epicenters; magnitudes higher than 3.0 are marked by large symbols. Temporal evolution of the relocated 2018 earthquake cluster is shown by the color scale. Events shallower than 2 km are marked by a black circle. Focal mechanism solutions (numbers 1–7) are shown. See Table S2 in Supporting Information S1 for additional details. An area of shallow active normal faults mapped by Tibor et al. (2004) is marked by the green grid-like hatch. Active deformed area proposed by Gasperini et al. (2020) is marked by slant lines in a gray oval. The postulated horsetail activated faults are marked in dashed black lines. Faults inferred from lineaments of the dip curvature residual gravity anomaly are in blue dashed lines (following Rosenthal et al., 2019).

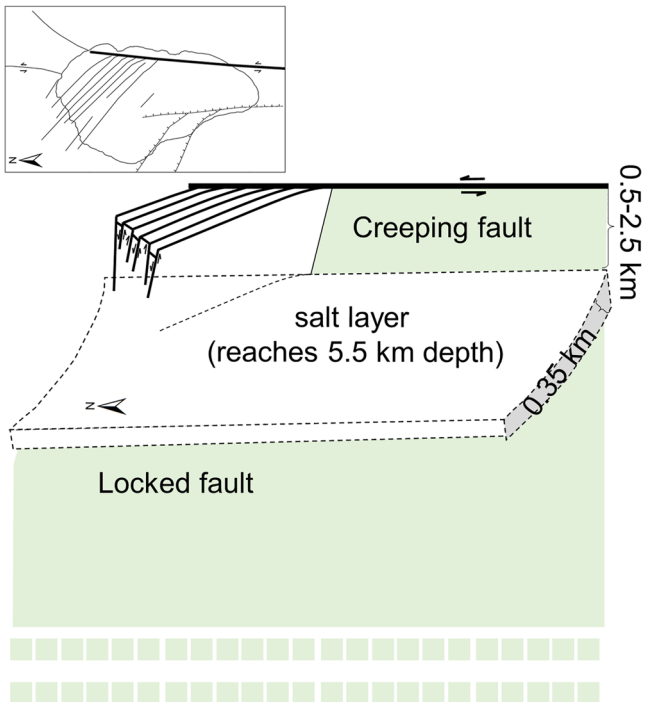

Figure 4. Schematic illustration of the horsetail normal faults at the tip of the Jordan Valley Fault (inspired by Courjault-Radé et al., 2009). Slip type, depth, and thickness data are from Hamiel et al. (2016) and Rosenthal et al. (2019). North is oriented to the left.

(Haddad et al., 2020). Consequently, the upper 0.5 km depth relocated hypocenters are probably inaccurate. The location error is ±3 km, which places the earthquakes at a possible depth of even approximately 4 km.

4. Discussion

The majority of the earthquakes in the two clusters form a NW-SE belt within a highly deformed area in the northern reaches of Lake Kinneret. The two swarms' locations, mechanisms of the larger earthquakes, and the shallow hypocenter depths, all imply a common seismo-tectonic mechanism. The parallelism between the inferred strikes of fault planes and the elongation of the belt argues for "horsetail" normal NW-SE faults splaying from the tip of the Jordan Valley Fault (Figure 3b dashed black lines). The epicenters appear to be bounded from the east (Figure 3b), probably by the Jordan Valley Fault (Haddad et al., 2020), implying the connection. Horsetail fractures are curved fault-lets splaying from the tip of a fault (e.g., Cunningham & Mann, 2007) (Figure 4). Supportive evidence for a horsetail structure comes from short-wavelength gravity anomaly maps (figure 13 in Rosenthal et al., 2019): a set of parallel lineaments runs within Lake Kinneret from the submerged Jordan Valley Fault to the northwest (Figure 3b). A few epicenters lie southwest of the earthquake belt, they are probably related to the horsetail structure of the Degania Fault (Figure 3b).

Similar horsetail normal faults, splaying from a strike-slip main fault, have been observed on a spectrum of scales, in the field, and in laboratory analogs (e.g., Gürboğa, 2016; Kim & Sanderson, 2006). Al-Taj (2000) discovered transtensional horsetail features in the Lower Jordan Valley in Ghor Kabid (north of the Dead Sea) (Figure 1). Recently, Al Hseinat et al. (2020) described contractional horsetail structures northeast of the Dead Sea. The Armutlu peninsula (northwest Turkey) provides another Middle-East example: horsetail fault splays from a dominant normal fault in a pull-apart at the tip of the Northern Anatolian Fault Zone (Kinscher et al., 2013).

Earlier earthquakes recorded by the ISN were located in the area of the 2013 and 2018 clusters (Figure 2b). Navon (2011) located >100 micro-earthquakes from 2010 in the same area; the majority are shallow (0–5 km depth), similar to the 2013 and 2018 clusters, implying of a common seismo-tectonic mechanism. Tibor et al. (2004) mapped shallow active normal faults along the northwestern margin with chirp seismic profiles and side-scan sonar (Figure 3b); some faults are parallel to the NW-SE fault belt and others perpendicular. Reznikov et al. (2004) and Gasperini et al. (2020) also suggested that the northwestern area is highly deformed.

Seismic studies in the lake did not identify the suggested horsetail faults. Hurwitz et al. (2002) and Reznikov et al. (2004) mapped NW-SE segments southwest of the earthquake belt (Figures 2c and 2d). It is possible that due to acoustic disruption of seismic images in gas-rich sediments, the faults were missed (Ben-Gai, 2011; Lazar et al., 2019; Reshef et al., 2007).

Gasperini et al. (2020), Haddad et al. (2020), and Wetzler et al. (2019) suggested that the clusters are swarms. Swarm activity may be induced by various processes, such as migration of magmatic/hydrothermal fluid (e.g., Dahm et al., 2008), tectonic activity (e.g., Llenos et al., 2009; Roland & McGuire, 2009), or anthropogenic activity, such as mining and fluid pumping (e.g., Wetzler et al., 2019). The triggering mechanism can also be a combination of these factors (e.g., Dublanchet & De Barros, 2020; Wei et al., 2015; Zhu et al., 2020). Here, we focus on a tectonic explanation. After presenting the proposal, we test the hypothesis and finally discuss previous mechanisms that have been proposed. Recent geodetic measurements across the Jordan Valley Fault, on a southern tangent of Lake Kinneret, indicate lateral creep of 2.5 ± 0.8 mm/year from the surface down to a depth of 1.5 ± 1.0 km, over a approximately 40 km distance (Hamiel et al., 2016; Hamiel & Piatibratova, 2021). A factor promoting slow slip could be a buried salt layer, as suggested for the Jordan Valley Fault by Hamiel et al. (2016). Under sufficient pressure (<30 MPa) and temperature (<200°C), the rheology of rocksalt transforms from brittle to ductile (Chen et al., 1997; Yang et al., 1999). Likewise, a decrease in slip rate at room temperature promotes

ductility (Shimamoto, 1986). We propose that the swarms express the release of energy accumulated in the interaction between the Jordan Valley creeping fault and the locked Jordan Gorge Fault north of it. The creeping fault induces swarms from time to time at the shallower part of the horsetail faults. For example, the 2010 earthquakes recorded by Navon (2011) (Figure 2b).

A thick evaporitic sequence was identified between depths of 1.3–3.8 km in the Zemah-1 well (Marcus & Slager, 1985), approximately 2 km south of Lake Kinneret (Figure 3b). Gravity data were modeled with the evaporitic layer reaching a depth of approximately 5 km under Lake Kinneret (Rosenthal et al., 2019) (Figure 2a). The salt-rich formation is presumed to be ductile, especially given the high thermal gradients (Shalev et al., 2013) beneath Pliocene basalt flows under Lake Kinneret (Ben-Avraham et al., 1980; Ginzburg & Ben-Avraham, 1986).

The evaporitic sequence may also be close to plastic yielding due to dipping subsurface. Two depocenters were detected in the southeast and northeast Lake Kinneret, near the creeping strand (Figure 2c), by gravity (Ben-Avraham et al., 1996) and seismic studies (Ben-Gai, 2011; Hurwitz et al., 2002; Reznikov et al., 2004). Based on Rosenthal et al.'s (2019) model, the dipping evaporitic formation near Lake Kinneret margins reaches approximately 3 km depth, consistent with the shallow creeping fault.

Shallow salt flow was also suggested as an inducer of fault creep in the Dead Sea (Hamiel & Piatibratova, 2021). It has also been suggested by Barnhart and Lohman (2013) in the Zagros mountains of Iran; a 1–2 km thick salt unit at 10–12 km depth is considered an inducer for creep in the sedimentary layers above it. Amri et al. (2021) described a pull-apart structure in the Northern Tunisian Atlas inverted to the ambient compressional stress regime. Mesozoic E-W local extension formed a pull-apart basin over a left step. Evaporitic deposition in the pull-apart was followed by thinning. Although the change in the stress regime is complex compared to our case study, it is still possible to identify many similarities at the early stages of formation. The step-over pull-apart structures are of similar scale, a prominent salt moderates the tectonics, and horsetail fault controls the extensional aspect of the basin. In the Atlas case, tectonic inversion to convergence is expressed by thrusting across what seems to have been originally normal faults with a horsetail pattern.

4.1. Testing the Hypothesis: A Coulomb Stress Change Model

We model the Coulomb stress change to evaluate cumulative slip from the interactions between the Jordan Valley Fault and the Jordan Gorge Fault that could induce the earthquake swarms.

4.1.1. Establishing the Model and Basic Assumptions

Gasperini et al. (2020) proposed a high-resolution fault map of Lake Kinneret (Figure 2e). They based their model on a particular selection from previous studies, without reference some to key studies (e.g., Ben-Gai, 2011; Hamiel et al., 2016; Heimann & Ron, 1993). The geometrical fault structure proposed by Gasperini et al. (2020) relies mostly on reprocessing and reinterpreting acoustic data, but disruptions could be misleading and cause misinterpretation (e.g., Ben-Gai, 2011; Lazar et al., 2019). Previous studies mapped a NE-SW deep-seated fault in the northwest Lake Kinneret from seismic (KNF, Figure 2c), steep gravity gradients, and short-wave magnetic anomalies (Ben-Avraham & ten Brink, 1989; Ben-Avraham et al., 1980; Hurwitz et al., 2002; Sneh & Weinberger, 2014), inconsistent with the CT interpretation (Figure 2e). Dembo et al. (2021) presented a model of the step-over in Lake Kinneret, based on paleomagnetic and geodetic research, indicating an active transform only on the east of Lake Kinneret. According to our results and Rosenthal et al.'s (2019) gravity lineaments, NW-SE striking faults are located west of the Jordan Valley Fault (Figure 3b), crossing the putative CT. Similar shallow NW-SE faults were also mapped onshore, on the Korazim Heights (Belitzky, 1987; Heimann & Ron, 1993; Rotstein & Bartov, 1989; Sneh, 2014a) with no evidence for the onshore CT continuation. To conclude, our tectonic model includes faults that are constrained by a number of methods (seismic, geodetic, and geological) and are compatible with studies of the area surrounding Lake Kinneret.

We use an elliptic slip distribution along the creeping fault for the stress change model, corresponding to a simple crack in an elastic medium (e.g., Dieterich & Smith, 2009). The cumulative stress due to the interaction of the creeping fault with the locked fault over time is equivalent in effect to a mainshock rupture with the same fault orientation and slip. Assuming that the creep rate over the last thousand years is constant and is 2.5 ± 0.8 mm/year, the accumulated stress is equivalent to a Mw 6.3 mainshock (Hamiel et al., 2016). This earthquake is conceptual (the accumulated stress might be different) in order to highlight lobes of stress distribution.

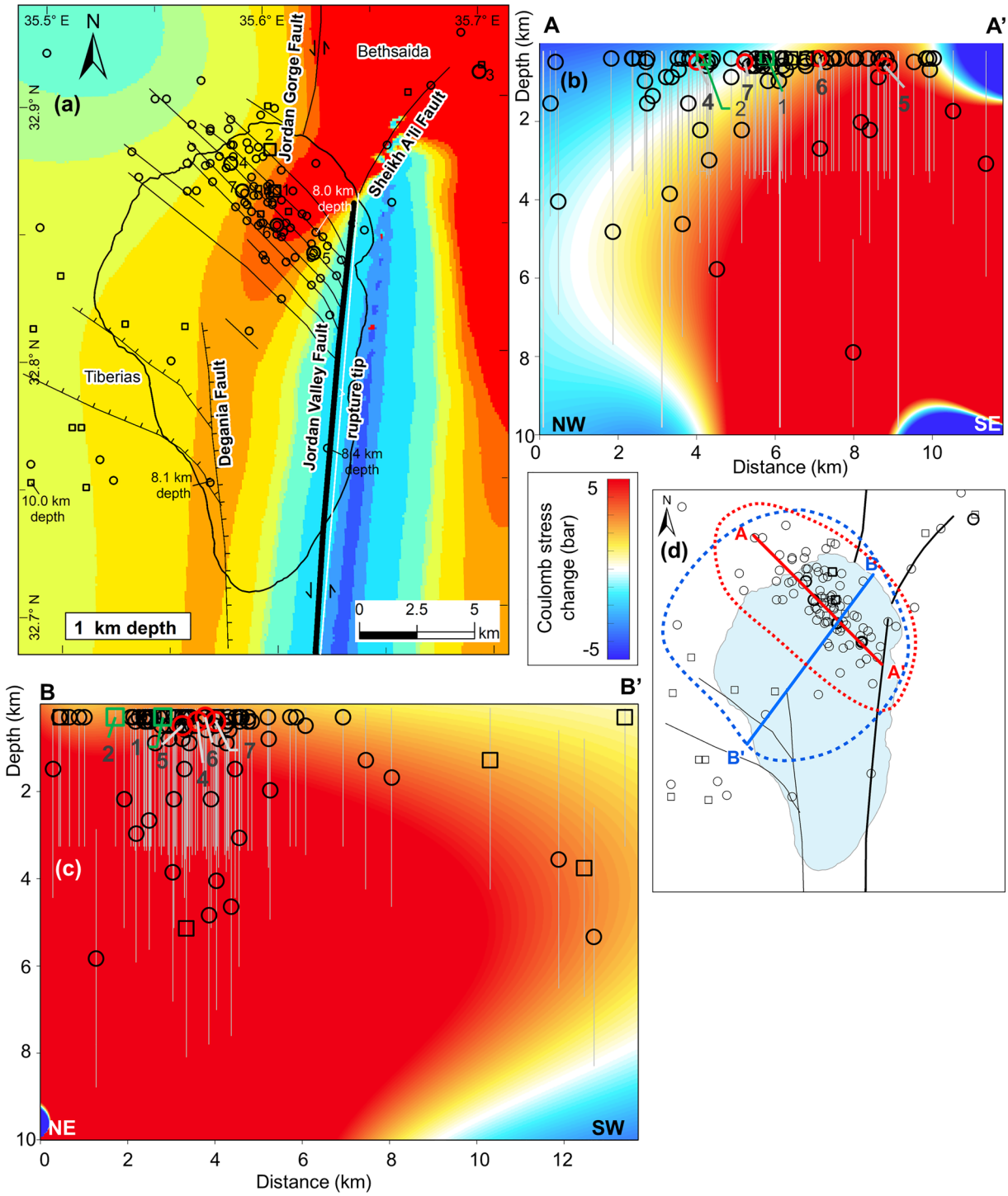

Figure 5. (a) Depth slice of 1 km calculated Coulomb stress change in Lake Kinneret. The 2013 (rectangles) and 2018 (circles) relocated hypocenters are marked. The seven largest earthquakes are in bold. (b)–(c) Coulomb stress change cross-sections. The seven larger earthquakes (no. 1–7) are colored. (b) A–A' cross-section (NW-SE direction). The larger earthquakes are marked. A depth error of ±3 km is estimated as in Grigoli et al. (2013). (c) B–'B' cross-section (NE-SW direction). (d) A map showing the location of the cross-sections. The earthquakes in the dashed red polygon are projected in (b). The earthquakes in the blue polygon are projected in (c).

We also assume that the creep on the Jordan Valley Fault continues northwards (offshore, totaling a approximately 60 km long segment) and decays toward the northern margin of the basin, where the salt formation tapers out (Rosenthal et al., 2019) (Figures 2a and Figure 5a bold line). We add to the model the accumulated slip from

the 4 mm/year slip rate of the transform faults (Hamiel et al., 2016). The accumulated slip is considered since the last known historic earthquake: 1033 CE on the Jordan Valley Fault and 1837 CE (or 1759 Figure S8 in Supporting Information S1) on the Jordan Gorge Fault (Agnon, 2014). The model assumes uniform stiffness, whereas a more realistic model might predict basal slip across the salt formation, focusing normal fault activity to the lake.

4.1.2. Stress Distribution

The stress maps in Figure 5 display lobes of relatively high probability for earthquakes (positive calculated Coulomb stress changes) in warm colors, while lower probability zones are shown in cold colors. Since most hypocenters occur in the shallow subsurface, the average depth is 1.2 km (Table S1 in Supporting Information S1), stresses at 1 km depth are shown in Figure 5a. Relatively high stress localized to the earthquake belt, with maximum values at the center, where the 2018 cluster initiated (Figure 3b). We suggest that the early and stronger shocks in the swarm triggered the peripheral earthquakes. More positive stress zones are located northeast of the belt—at the Bethsaida Valley and on the Sheikh A'li Fault, where some of the earthquakes were relocated.

Projections on cross-sections of the calculated stress field show preference of foci to the stressed zone. A NW-SE cross-section (Figure 5b), parallel to the earthquake belt, is relatively densely populated with foci at the center of the section, where the 2018 cluster initiated (Figure 3b). As suggested, the peripheral earthquakes may have been triggered by the former earthquakes. A NE-SW cross-section (Figure 5c) is also consistent with our hypothesis, the probability of earthquakes at shallow depths is relatively high. The positive stress lobe covers most of the earthquake belt and expands southwest to the Degania Fault. The positive lobe is consistent with the suggested horsetail faults (based on the gravity lineaments) expanding south (Figure 3b), and a few earthquakes relocated to the Degania Fault area (Figures 5a and 5c). Stress is more concentrated under the transform strands (the Jordan Valley Fault and the Jordan Gorge Fault) beneath the creeping depth. The stress distribution implies that deeper tectonic processes dominate at that depth, following the accumulated slip below the locking depth.

4.1.3. Other\Complementary Hypotheses

Wetzler et al. (2019) proposed a poroelastic mechanism for triggering the clusters. Our present hypothesis focuses on the tectonic loads and does not exclude a combination of factors (tectonic creep and pore pressure change).

Haddad et al. (2020) suggested that deep fluids triggered the swarms on putative segments of the transform fault. The hypothesis is based on Gasperini et al.'s (2020) proposal, identifying a mantle source for fluid samples around Lake Kinneret. They conclude that the fluids might be connected to magmatic intrusions at depth or linked to the mantle-crust boundary. This hypothesis is yet to be corroborated: magmatism in the area has been going on and off, some magmatic vents were shut off for 4 million years before reactivation (e.g., Baer et al., 2006), so we do not rule out an active magmatic source. However, none of the fluid samples were taken under the epicentral area. Torfstein et al. (2013) also detected the fluids but attributed them to young, probably shallow, volcanic activity rather than a direct deep root. In addition, as we show, the well-developed surface waves characterize shallow earthquakes (Figure S4 in Supporting Information S1). Also, our depth calculations, using several methods and a number of velocity models (Tables S1–S4, Figures S1–S3, S5–S7 in Supporting Information S1), indicate shallow foci, again implying a shallow inducer.

5. Conclusions

We present a new hypothesis to explain the July–August 2018 earthquake swarm and its October 2013 precursor in Lake Kinneret. Ductile behavior of a buried salt-rich formation (which reaches a few kilometers depth) promotes creep on the Jordan Valley Fault. Hamiel et al. (2016) detected fault creep from the surface down to a depth of 1.5 ± 1.0 km in the southern Lake Kinneret. We assume that the fault creep extends north, up to the area of the 2018 swarm. This assumption is consistent with Rosenthal et al.'s (2019) gravimetric results, where the salt formation underlies the entire Lake Kinneret and tapers out sharply outside the basin. We relocated the earthquakes and calculated the mechanism of the larger earthquakes using several methods and velocity models. According to our calculations, the earthquakes are shallow, the majority $\leq$6 km depth. The larger earthquakes were emitted from normal faults, striking NW-SE. We suggest the earthquakes ruptured NW-SE shallow faults forming a horsetail pattern off the tip of the Jordan Valley Fault. Lineaments in the short-wavelength

gravity-anomaly published map support horsetail faults. We test our hypothesis by calculating Coulomb stress change and show that the stress distribution is consistent with earthquake locations.

Data Availability Statement

Supporting information available at: https://www.neev-center.com/_files/ugd/70b2b4_4e4451a2d5bf48bba7c-5c93da9943fcb.pdf.

Acknowledgments
The authors are especially grateful to Dr. John K. Hall, founder of Neev's Center for Geoinfomatics, for his ongoing support and to Dr. Yaacov Arkin and Inga Boianju for reviewing earlier versions of the manuscript. The study was supported by the Ministry of Energy (grant number # 45/2019); the German-Israel Foundation for Scientific Research and Development (grant number # I-1280-301.8); and the Israel Science Foundation (grant number ISF # 2091/20).

References

Agnon, A. (2014). Pre-instrumental earthquakes along the Dead Sea Rift. In Z. Garfunkel, Z. Ben-Avraham, & E. Kagan (Eds.). *Dead Sea transform fault system: Reviews* (6th ed., pp. 207–261). Springer. https://doi.org/10.1007/978-94-017-8872-4_8

Al Hseinat, M., Al-Rawabdeh, A., Al-Zidaneen, M., Ghanem, H., Al-Taj, M., Diabat, A., et al. (2020). New insights for understanding the structural deformation style of the strike-slip regime along the Wadi Shueib and Amman-Hallabat structures in Jordan based on remote sensing data analysis. *Geosciences*, *10*(7), 1–22. https://doi.org/10.3390/geosciences10070253

Al-Taj, M. M. I. (2000). *Active faulting along the Jordan valley segment of the Jordan–Dead Sea transform (Doctoral dissertation)*. The University of Jordan (theses.ju.edu.jo).

Ambraseys, N. N. (1997). The earthquake of 1 January 1837 in southern Lebanon and Northern Israel. *Annali Di Geofisica*, *XL*(4), 923–935. Retrieved from http://hdl.handle.net/2122/1595

Ambraseys, N. N., & Barazangi, M. (1989). The 1759 earthquake in the Bekaa Valley: Implications for earthquake hazard assessment in the eastern Mediterranean region. *Geophysical Research*, *94*(B4), 4007–4013. https://doi.org/10.1029/JB094iB04p04007

Ambraseys, N. N., & Jackson, J. A. (1998). Faulting associated with historical and recent earthquakes in the Eastern Mediterranean region. *Geophysical Journal International*, *133*(2), 390–406. https://doi.org/10.1046/j.1365-246X.1998.00508.x

Amri, Z., Masrouhi, A., Naji, C., Bellier, O., & Koyi, H. (2021). Mechanical relationship between strike-slip faulting and salt tectonics in the Northern Tunisian Atlas: The Bir-El-Afou salt structure. *Journal of Structural Geology*, *154*(June 2021), 104501. https://doi.org/10.1016/j.jsg.2021.104501

Baer, G., Aharon, L., Heimann, A., Shaliv, G., & Agnon, A. (2006). The Nahal Tavor vent: Interplay of Miocene tectonics, dikes, and volcanism in the lower Galilee, Israel. *Israel Journal of Earth Sciences*, *55*(1), 1–15. https://doi.org/10.1560/ijes_55_1_1

Barnhart, W. D., & Lohman, R. B. (2013). Phantom earthquakes and triggered aseismic creep: Vertical partitioning of strain during earthquake sequences in Iran. *Geophysical Research Letters*, *40*(5), 819–823. https://doi.org/10.1002/grl.50201

Bartov, Y., Steinitz, G., Eyal, M., & Eyal, Y. (1980). Sinistral movement along the Gulf of Aqaba - Its age and relation to the opening of the Red Sea. *Nature*, *285*, 220–222. https://doi.org/10.1038/285220a0

Belitzky, S. (1987). *Tectonics of the Korazim saddle (master's thesis)*. The Hebrew University, Jerusalem. Retrieved from https://libraries.huji.ac.il/Harman

Ben-Avraham, Z. (1985). Structural framework of the Gulf of Elat (Aqaba)—Northern Red Sea. *Journal of Geophysical Research*, *90*, 703–726. https://doi.org/10.1029/JB090iB01p00703

Ben-Avraham, Z., Shoham, Y., Klein, E., Michelson, H., & Serruya, C. (1980). Magnetic survey of Lake Kinneret - Central Jordan valley, Israel. *Marine Geophysical Researches*, *4*, 257–276. https://doi.org/10.1007/BF00369102

Ben-Avraham, Z., & ten Brink, U. (1989). Transverse faults and segmentation of basins within the Dead Sea Rift. *Journal of African Earth Sciences*, *8*(2–4), 603–616. https://doi.org/10.1016/S0899-5362(89)80047-8

Ben-Avraham, Z., ten Brink, U., Bell, R., & Reznikov, M. (1996). Gravity field over the Sea of Galilee: Evidence for a composite basin along a transform fault. *Journal of Geophysical Research: Solid Earth*, *101*(B1), 533–544. https://doi.org/10.1029/95JB03043

Ben-Gai, Y. (2011). Subsurface geology of the southern Lake Kinneret (Sea of Galilee), Dead Sea transform - evidence from seismic reflection data. *Israel Journal of Earth Sciences*, *58*(3), 163–175. https://doi.org/10.1560/ijes.58.3-4.163

Cesca, S., Heimann, S., Stammler, K., & Dahm, T. (2010). Automated procedure for point and kinematic source inversion at regional distances. *Geophysical Research*, *115*, 1–24. https://doi.org/10.1029/2009JB006450

Chen, Z., Wang, M. L., & Lu, T. (1997). Study of tertiary creep of rock salt. *Journal of Engineering Mechanics*, *123*(1), 77–82. https://doi.org/10.1061/(asce)0733-9399(1997)123:1(77)

Courjault-Radé, P., Darrozes, J., & Gaillot, P. (2009). The M = 5.1 1980 Arudy earthquake sequence (western Pyrenees, France): A revisited multi-scale integrated seismologic, geomorphologic and tectonic investigation. *International Journal of Earth Sciences*, *98*(7), 1705–1719. https://doi.org/10.1007/s00531-008-0320-5

Cunningham, W. D., & Mann, P. (2007). Tectonics of strike-slip restraining and releasing bends. *Geological Society, London, Special Publication*, *290*, 1–12. https://doi.org/10.1144/SP290.1

Dahm, T., Fischer, T., & Hainzl, S. (2008). Mechanical intrusion models and their implications for the possibility of magma-driven swarms in NW Bohemia Region. *Studia Geophysica et Geodaetica*, *52*(4), 529–548. https://doi.org/10.1007/s11200-008-0036-9

Dembo, N., Hamiel, Y., & Granot, R. (2021). The stepovers of the Central Dead Sea Fault: What can we learn from the confining vertical axis rotations? *Tectonophysics*, *816*(August), 229036. https://doi.org/10.1016/j.tecto.2021.229036

Dieterich, J. H., & Smith, D. E. (2009). Nonplanar faults: Mechanics of slip and off-fault damage. *Pure and Applied Geophysics*, *166*(10–11), 1799–1815. https://doi.org/10.1007/s00024-009-0517-y

Dublanchet, P., & De Barros, L. (2020). Dual seismic migration velocities in seismic swarms. *Geophysical Research Letters*, *47*, 1–10. https://doi.org/10.1029/2020GL090025

Duman, T. Y., & Emre, Ö. (2013). The East Anatolian Fault: Geometry, segmentation and jog characteristics. *Geological Society, London, Special Publication*, *372*(1), 495–529. https://doi.org/10.1144/SP372.14

Ellenblum, R., Marco, S., Agnon, A., Rockwell, T., & Boas, A. (1998). Crusader castle torn apart by earthquake at dawn, 20 May 1202. *Geology*, *26*(4), 303–306. https://doi.org/10.1130/0091-7613(1998)026<0303:cctabe>2.3.co;2

Ellenblum, R., Marco, S., Kool, R., Davidovitch, U., Porat, R., & Agnon, A. (2015). Archaeological record of earthquake ruptures in Tell Ateret, the Dead Sea fault. *Tectonics*, *34*(10), 2105–2117. https://doi.org/10.1002/2014TC003815

Eppelbaum, L., Ben-Avraham, Z., & Katz, Y. (2007). Structure of the Sea of Galilee and Kinarot valley derived from combined geological-geophysical analysis. *First Break*, 25(1), 43–50. https://doi.org/10.3997/1365-2397.2007001

Feigin, G., & Shapira, A. (1994). A unified crustal model for calculating travel times of seismic waves across the Israel Seismic Network. In *The institute of petroleum research and geophysics report. Z1/567/79* (Vol. *107*, pp. 1–14).

Ferrario, M. F., Katz, O., Hillman, A., Livio, F., Amit, R., & Michetti, A. M. (2020). The mid-eighth century CE surface faulting along the Dead Sea fault at Tiberias (Sea of Galilee, Israel). *Tectonics*, *39*(9), 1–21. https://doi.org/10.1029/2020TC006186

Ferry, M., Meghraoui, M., Karaki, N. A., Al-Taj, M., & Khalil, L. (2011). Episodic behavior of the Jordan Valley section of the Dead Sea Fault inferred from a 14-ka-long integrated catalog of large earthquakes. *Bulletin of the Seismological Society of America*, *101*(1), 39–67. https://doi.org/10.1785/0120100097

Freed, A. M. (2005). Earthquake triggering by static, dynamic, and postseismic stress transfer. *Annual Review of Earth and Planetary Sciences*, *33*(1), 335–367. https://doi.org/10.1146/annurev.earth.33.092203.122505

Freund, R., Garfunkel, Z., Zak, I., Goldberg, M., Weissbrod, T., & Derin, B. (1970). The shear along the Dead Sea rift. *Philosophical Transactions for the Royal Society of London. Series A, Mathematical and Physical Sciences*, *267*, 107–130. https://doi.org/10.1098/rsta.1970.0027

Garfunkel, Z. (1981). Internal structure of the Dead Sea Leaky Transform (rift) in relation to plate kinematics. *Tectonophysics*, *80*(1–4), 81–108. https://doi.org/10.1016/0040-1951(81)90143-8

Garfunkel, Z., Zak, I., & Freund, R. (1981). Active faulting in the Dead Sea rift. *Tectonophysics*, *80*, 1–26. https://doi.org/10.1016/0040-1951(81)90139-6

Gasperini, L., Lazar, M., Mazzini, A., Lupi, M., Haddad, A., Hensen, C., et al. (2020). Neotectonics of the Sea of Galilee (northeast Israel): Implication for geodynamics and seismicity along the Dead Sea fault System. *Scientific Reports*, *10*, 11932. https://doi.org/10.1038/s41598-020-67930-6

Ginzburg, A., & Ben-Avraham, Z. (1986). Structure of the Sea of Galilee graben, Israel, from magnetic measurements. *Tectonophysics*, *126*, 153–164. https://doi.org/10.1016/0040-1951(86)90225-8

Gitterman, Y., Pinsky, V., Shapira, A., Ergin, M., Kalafat, D., Gurbuz, G., & Solomi, K. (2002). Improvement in detection, location and identification of small events through joint data analysis by seismic stations in the Middle East/Eastern Mediterranean region. *Proceedings of the 24th Seismic Research Review Nuclear Explosion Monitoring: Innovation and Integration*. (pp. 271–282). DTRA01-00-C-0119.

Grigoli, F., Cesca, S., Vassallo, M., & Dahm, T. (2013). Automated seismic event location by travel-time stacking: An application to mining induced seismicity. *Seismological Research Letters*, *84*(4), 666–677. https://doi.org/10.1785/0220120191

Gürboğa, Ş. (2016). The termination of the North Anatolian Fault system (NAFS) in eastern Turkey. *International Geology Review*, *58*(12), 1557–1567. https://doi.org/10.1080/00206814.2016.1175976

Haddad, A., Alcanie, M., Zahradník, J., Lazar, M., Antunes, V., Gasperini, L., et al. (2020). Tectonics of the Dead Sea fault driving the July 2018 seismic swarm in the Sea of Galilee (Lake Kinneret), Israel. *Journal of Geophysical Research: Solid Earth*, *125*(10), 1–14. https://doi.org/10.1029/2019jb018963

Hamiel, Y., & Piatibratova, O. (2021). Spatial variations of slip and creep rates along the southern and central Dead Sea fault and the Carmel–Gilboa fault system. *Journal of Geophysical Research: Solid Earth*, *126*(9), 1–17. https://doi.org/10.1029/2020JB021585

Hamiel, Y., Piatibratova, O., & Mizrahi, Y. (2016). Creep along the northern Jordan valley section of the Dead Sea fault. *Geophysical Research Letters*, *43*(6), 2494–2501. https://doi.org/10.1002/2016GL067913

Heimann, A., & Ron, H. (1993). Geometric changes of plate boundaries along part of the northern Dead Sea transform: Geochronologic and paleomagnetic evidence. *Tectonics*, *12*(2), 477–491. https://doi.org/10.1029/92TC01789

Heimann, S., Isken, M., Kühn, D., Sudhaus, H., Steinberg, A., Vasyura-Bathke, H., et al. (2018). *Grond - a probabilistic earthquake source inversion framework. V. 1.0*. GFZ Data Services. https://doi.org/10.5880/GFZ.2.1.2018.003

Hofstetter, R., Klinger, Y., Amrat, A. Q., Rivera, L., & Dorbath, L. (2007). Stress tensor and focal mechanisms along the Dead Sea fault and related structural elements based on seismological data. *Tectonophysics*, *429*(3–4), 165–181. https://doi.org/10.1016/j.tecto.2006.03.010

Hough, S. E., & Avni, R. (2011). The 1170 and 1202 CE Dead Sea rift earthquakes and long-term magnitude distribution of the Dead Sea Fault Zone. *Israel Journal of Earth Sciences*, *58*, 295–308. https://doi.org/10.1560/IJES.58.3-4.295

Hurwitz, S., Garfunkel, Z., Ben-Gai, Y., Reznikov, M., Rotsteina, Y., & Gvirtzman, H. (2002). The tectonic framework of a complex pull-apart basin: Seismic reflection observations in the Sea of Galilee, Dead Sea Transform. *Tectonophysics*, *359*, 289–306. https://doi.org/10.1016/S0040-1951(02)00516-4

Kearey, P., Brooks, M., & Hill, I. (2002). *Elements of seismic surveying. An introduction to geophysical exploration*. (pp. 24–25). Blackwell Science Ltd.

Kim, Y. S., & Sanderson, D. J. (2006). Structural similarity and variety at the tips in a wide range of strike-slip faults: A review. *Terra Nova*, *18*(5), 330–344. https://doi.org/10.1111/j.1365-3121.2006.00697.x

King, G. C. P., Stein, R. S., & Jian, L. (1994). Static stress changes and the triggering of earthquakes. *Bulletin of the Seismological Society of America*, *84*(3), 935–953. https://doi.org/10.1785/BSSA0840030935

Kinscher, J., Krüger, F., Woith, H., Lühr, B. G., Hintersberger, E., Irmak, T. S., & Baris, S. (2013). Seismotectonics of the Armutlu peninsula (Marmara Sea, NW Turkey) from geological field observation and regional moment tensor inversion. *Tectonophysics*, *608*, 980–995. https://doi.org/10.1016/j.tecto.2013.07.016

Lazar, M., Gasperini, L., Polonia, A., Lupi, M., & Mazzini, A. (2019). Constraints on gas release from shallow lake sediments—A case study from the Sea of Galilee. *Geo-Marine Letters*, *39*(5), 377–390. https://doi.org/10.1007/s00367-019-00588-w

Llenos, A. L., McGuire, J. J., & Ogata, Y. (2009). Modeling seismic swarms triggered by aseismic transients. *Earth and Planetary Science Letters*, *281*(1–2), 59–69. https://doi.org/10.1016/j.epsl.2009.02.011

Marco, S., Agnon, A., Ellenblum, R., Eidelman, A., Basson, U., & Boas, A. (1997). 817-year-old walls offset sinistrally 2.1 m by the Dead Sea Transform, Israel. *Journal of Geodynamics*, *24*(1–4), 11–20. https://doi.org/10.1016/S0264-3707(96)00041-5

Marco, S., Hartal, M., Hazan, N., Lev, L., & Stein, M. (2003). Archaeology, history, and geology of the A.D. 749 earthquake, Dead Sea transform. *Geology*, *31*(8), 665–668. https://doi.org/10.1130/G19516.1

Marco, S., Rockwell, T. K., Heimann, A., Frieslander, U., & Agnon, A. (2005). Late Holocene activity of the Dead Sea transform revealed in 3D palaeoseismic trenches on the Jordan Gorge segment. *Earth and Planetary Science Letters*, *234*(1–2), 189–205. https://doi.org/10.1016/j.epsl.2005.01.017

Marcus, E., & Slager, J. (1985). The sedimentary-magmatic sequence of the Zemah-1 well (Jordan– Dead Sea rift, Israel) and its emplacement in time and space. *Israel Journal of Earth Sciences*, *34*(1), 1–10.

Meiler, M., Reshef, M., & Shulman, H. (2011). Seismic depth-domain stratigraphic classification of the Golan Heights, central Dead Sea fault. *Tectonophysics*, *510*(3–4), 354–369. https://doi.org/10.1016/j.tecto.2011.08.007

Michelson, H. (1972). *The hydrogeology of the southern Golan Heights (Rep. HR/72/037)*. Tahal—Water Planning for Israel Ltd.

Navon, H. (2011). *Microseismic characterization of Lake Kinneret Basin (master's thesis)*. Tel-Aviv University, Israel. Retrieved from www.researchgate.net

Reshef, M., Ben-Avraham, Z., Tibor, G., & Marco, S. (2007). The use of acoustic imaging to reveal fossil fluvial systems-a case study from the southwestern Sea of Galilee. *Geomorphology*, *83*(1–2), 58–66. https://doi.org/10.1016/j.geomorph.2006.05.017

Reznikov, M., Ben-Avraham, Z., Garfunkel, Z., Gvirtzman, H., & Rotsteina, Y. (2004). Structural and stratigraphic framework of Lake Kinneret. *Israel Journal of Earth Sciences*, *53*(3–4), 131–149. https://doi.org/10.1560/QY1W-VVRM-FLNK-C9M9

Roland, E., & McGuire, J. J. (2009). Earthquake swarms on transform faults. *Geophysical Journal International*, *178*(3), 1677–1690. https://doi.org/10.1111/j.1365-246X.2009.04214.x

Rosenthal, M., Ben-Avraham, Z., & Schattner, U. (2019). Almost a sharp cut – a case study of the cross point between a continental transform and a rift, based on 3D gravity modeling. *Tectonophysics*, *761*(November 2018), 46–64. https://doi.org/10.1016/j.tecto.2019.04.012

Rotstein, Y., & Bartov, Y. (1989). Seismic reflection across a continental transform: An example from a convergent segment of the Dead Sea Rift. *Journal of Geophysical Research*, *94*(B3), 2902–2912. https://doi.org/10.1029/JB094iB03p02902

Sade, A. R., Tibor, G., Hall, J. K., Diamant, M., Sade, H., Hartman, G., et al. (2009). Multibeam bathymetry of the Sea of Galilee (Lake Kinneret). In *The geological map of Israel in scale 1:33333*. Geological Survey of Israel. Oceanographic and Limnological Research H-16-2009, Geological Survey of Israel, (GSI/05/2009).

Sengör, A. M. C. (1979). the North Anatolian Transform Fault: Its age, offset and tectonic significance. *Journal of the Geological Society*, *136*(December 1939), 269–282. https://doi.org/10.1144/gsjgs.136.3.0269

Shalev, E., Lyakhovsky, V., Weinstein, Y., & Ben-Avraham, Z. (2013). The thermal structure of Israel and the Dead Sea fault. *Tectonophysics*, *602*, 69–77. https://doi.org/10.1016/j.tecto.2012.09.011

Sharon, M., Sagy, A., Kurzon, I., Marco, S., & Rosensaft, M. (2020). Assessment of seismic sources and capable faults through hierarchic tectonic criteria: Implications for seismic hazard in the Levant. *Natural Hazards and Earth System Sciences*, *20*(1), 125–148. https://doi.org/10.5194/nhess-20-125-2020

Shimamoto, T. (1986). Transition between frictional slip and ductile flow for halite shear zones at room temperature. *Science*, *231*(4739), 711–714. https://doi.org/10.1126/science.231.4739.711

Shulman, H., Reshef, M., & Ben-avraham, Z. (2004). The structure of the Golan Heights and its tectonic linkage to the Dead Sea transform and the Palmyrides folding. *Israel Journal of Earth Sciences*, *53*, 225–237. https://doi.org/10.1560/MWVC-CGPU-65KU-FFPY

Sneh, A. (2014a). Arbel (Sheet 4-I). In *The geological map of Israel in scale 1:50000*. Geological Survey of Israel.

Sneh, A. (2014b). Teverya (Sheet 4-II). In *The geological map of Israel in scale 1:50000*. Geological Survey of Israel.

Sneh, A., & Weinberger, R. (2014). *Major geological structures of Israel and environs, 1:500,000 scale*. Geological Survey of Israel.

Tibor, G., Ben-Avraham, Z., Herut, B., Nishri, A., & Zurielib, A. (2004). Bottom morphology and shallow structures in the northwestern part of Lake Kinneret. *Israel Journal of Earth Sciences*, *53*(3–4), 173–186. https://doi.org/10.1560/te15-ku60-6xv3-xk5u

Torfstein, A., Hammerschmidt, K., Friedrichsen, H., Starinsky, A., Garfunkel, Z., & Kolodny, Y. (2013). Helium isotopes in Dead Sea transform waters. *Chemical Geology*, *352*, 188–201. https://doi.org/10.1016/j.chemgeo.2013.06.008

Van-Eck, T., & Hofstetter, A. (1990). Fault geometry and spatial clustering of microearthquakes along the Dead Sea - Jordan Rift fault zone. *Tectonophysics*, *180*, 15–27. https://doi.org/10.1016/0040-1951(90)90368-I

Wechsler, N., Rockwell, T. K., Klinger, Y., Štěpančíková, P., Kanari, M., Marco, S., & Agnon, A. (2014). A paleoseismic record of earthquakes for the dead sea transform fault between the first and seventh centuries C.E: Nonperiodic behavior of a plate boundary fault. *Bulletin of the Seismological Society of America*, *104*(3), 1329–1347. https://doi.org/10.1785/0120130304

Wei, S., Avouac, J. P., Hudnut, K. W., Donnellan, A., Parker, J. W., Graves, R. W., et al. (2015). The 2012 Brawley swarm triggered by injection-induced aseismic slip. *Earth and Planetary Science Letters*, *422*, 115–125. https://doi.org/10.1016/j.epsl.2015.03.054

Wetzler, N., & Kurzon, I. (2016). The earthquake activity of Israel: Revisiting 30 years of local and regional seismic records along the Dead Sea transform. *Seismological Research Letters*, *87*(1), 47–58. https://doi.org/10.1785/0220150157

Wetzler, N., Shalev, E., Göbel, T., Amelung, F., Kurzon, I., Lyakhovsky, V., & Brodsky, E. E. (2019). Earthquake swarms triggered by groundwater extraction near the Dead Sea Fault. *Geophysical Research Letters*, *46*(14), 8056–8063. https://doi.org/10.1029/2019gl083491

Yang, C., Daemen, J. J. K., & Yin, J. H. (1999). Experimental investigation of creep behavior of salt rock. *International Journal of Rock Mechanics and Mining Sciences*, *36*(2), 233–242. https://doi.org/10.1016/S0148-9062(98)00187-9

Zhu, W., Allison, K. L., Dunham, E. M., & Yang, Y. (2020). Fault valving and pore pressure evolution in simulations of earthquake sequences and aseismic slip. *Nature Communications*, *11*(4833), 1–11. https://doi.org/10.1038/s41467-020-18598-z

References From the Supporting Information

Hudson, J. A., Pearce, R. G., & Rogers, R. M. (1989). Source type plot for inversion of the moment tensor. *Journal of Geophysical Research: Solid Earth*, *94*(B1), 765–774. https://doi.org/10.1029/JB094iB01p00765